AD-A135 946 OHMIC HEATING OF THE POLAR F-REGION BY HF (HIGH FREQUENCY) PULSE(U) CALIFORNIA UNIV LOS ANGELES CENTER FOR PLASMA PHYSICS AND FUS.. M M SHOUCRI ET AL. OCT 83 1/1

UNCLASSIFIED PPG-748 N00014-75-C-0476 F/G 4/1 NL

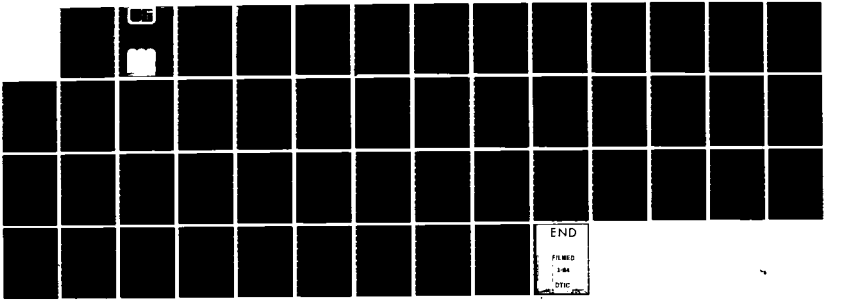

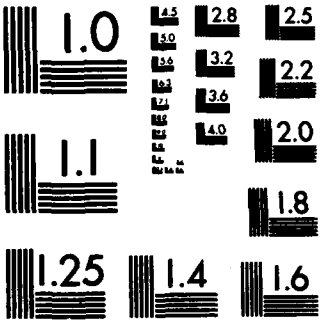

MICROCOPY RESOLUTION TEST CHART
NATIONAL BUREAU OF STANDARDS-1963-A

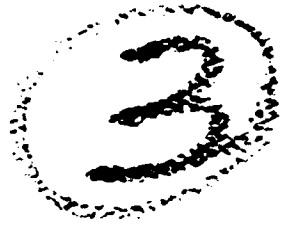

Ohmic Heating of the Polar F-Region by HF Pulse

M. M. Shoucri, G. J. Morales & J. E. Maggs

PPG-748 October, 1983

Contract N00014-75-C-0476

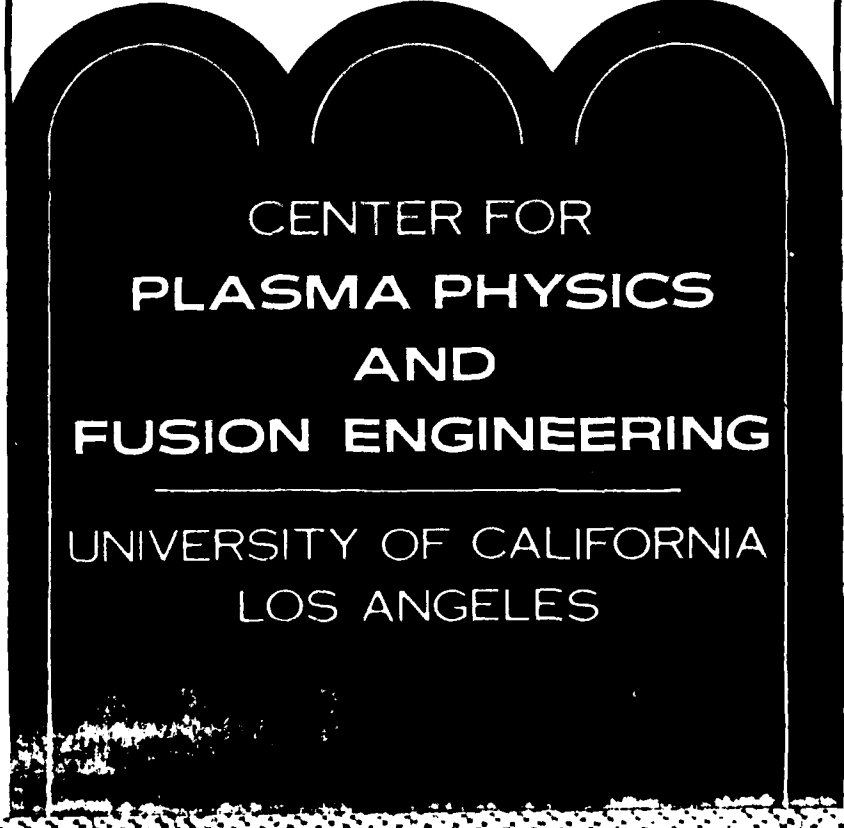

Ohmic Heating of the Polar F-Region by HF Pulse

M. M. Shoucri, G. J. Morales & J. E. Maggs

PPG-748 October, 1983

Contract N00014-75-C-0476

Department of Physics

University of California

Los Angeles, California 90024

-a-

Ohmic Heating of the Polar F-Region by HF Pulses

Merit M. Shoucri and G. J. Morales
Physics Department
University of California at Los Angeles
Los Angeles, California 90024

and

J. E. Maggs
Institute for Geophysics and Planetary Physics
University of California at Los Angeles
Los Angeles, California 90024

ABSTRACT

A study of the modifications produced by high power, high frequency (HF) waves in the F-region of a quiet (low solar cycle) polar ionosphere is presented. In the polar geometry, maximum Ohmic heating occurs producing significant changes to the zero order electron temperature and density profiles. The temporal and spatial aspects of these changes are calculated and their effects on relevant ionospheric parameters, such as the d.c. conductivity tensor, are found. An interesting finding is the generation of density cavities at the reflection point of the HF waves. A survey of the dependence of the various effects on HF pump parameters is made.

I. INTRODUCTION

Presently, there is renewed interest in the problem of ionospheric modification by high power HF waves. To a large extent this activity has been stimulated by the recent completion of versatile experimental facilities near the polar region, namely, HEATER in Norway [Stubbe et al., 1982] and HIPAS in Alaska [Wong et al., 1981]. Although the ionospheric modification problem has been extensively investigated over the past decade (see for reference, Vol. 9, issue No. 11, Radio Science [1974]; Vol. 44, issue No. 12, Journal of Atmospheric and Terrestrial Physics [1982]), the majority of theoretical and numerical investigations have been primarily directed to understanding processes of relevance to the mid-latitude ionosphere [Meltz and Lelevier, 1970; Meltz et al., 1974]. This is essentially because of the location of the earlier experimental facilities in Platteville, Colorado and Arecibo, Puerto Rico. Although some of the physical processes at work in mid-latitude ionospheric modification are also encountered in the polar region, the latter environment has certain unique features which demand specialized attention. With this perspective in mind, the present study aims to establish a background for the simplest study of ionospheric modification in the polar F-region, from which more sophisticated models can develop. It is hoped that this study may serve as a reference against which some of the ongoing experiments can be compared as well as a means of assessing the potential of future field studies.

Among the various unique features encountered in the polar ionosphere, the fact that the magnetic field of the earth makes a small angle with the plasma density gradient has a profound impact on the heating produced by HF waves. The reason is that the heating source (i.e., the HF beam) can be nearly colinear with the direction of the heat flow (i.e., parallel to the

magnetic field lines), resulting in enhanced heating along a magnetic flux tube. This situation is to be contrasted with a mid-latitude or equatorial heating geometry in which only a small portion of a flux tube is exposed to the HF beam. The results of the present investigation aim to emphasize the role of the colinear heating by concentrating on the case $\nabla N_{eo} \times \underline{B}_o = 0$, where N_{eo} is the zero order plasma density, and $\underline{B}_o$ the earth's magnetic field. Some interesting features of the colinear heating geometry have already been examined in the context of simulating microwave beam heating from power station satellites [Perkins and Roble, 1978]. A technical simplification which results from the consideration of the idealized $\nabla N_{eo} \times \underline{B}_o = 0$ geometry is that the spatial dependence of the HF electric field can be well represented analytically, thus permitting the consideration of overdense heating scenarios, i.e., heating below the critical frequency of the F-region (ωF_2). Enhanced absorption near the reflection layer, of great experimental interest [e.g., Gordon and Carlson, 1974; Mantas et al., 1981], is thus accurately calculated without recourse to the approximations necessary in mid-latitude studies [Thomson, 1970; Meltz et al., 1974]. Also, since in this geometry linear mode conversion and parametric decay instabilities are absent, the only heating channel is purely Ohmic (collisional). Therefore, by emphasizing this geometry one obtains an upper bound on the magnitude of the effects resulting from Ohmic heating.

The present spatial and temporal study of transport in a model polar ionosphere addresses only the changes produced in the F-region plasma. The complicating effects arising from the chemistry of the D and E-regions are best studied separately since they occur on different time scales, and are not sensitive to the unique $\nabla N_{eo} \times \underline{B}_o \approx 0$ polar geometry because of the low degree of

magnetization at lower heights. In addition, many of the experimental effects presently being studied take place in the F-region [e.g., Mantas et al., 1981; Stubbe et al., 1982]. Hence it is of importance to assess the role of collisional heating in this region.

In describing the interaction of HF heated electrons with the various neutral components, the present investigation incorporates the substantial body of knowledge available in this area; see for example Schunk and Nagy [1980] and the references therein. In particular, this work relies heavily on the works of Banks and Kockarts [1973] and Rees and Roble [1975] in evaluating the collision cross sections, the elastic and inelastic cooling losses, and the thermal conductivity.

The present investigation uses an analytic expression for the electric field of the HF pump valid for the polar F-region. The Ohmic absorption of this field is calculated, as well as the resulting absorption coefficient. The self-consistent evolution of the temperature and density variations is numerically calculated. Their feedback on relevant ionospheric parameters is found. A survey is made of the dependence on background density and on HF heater parameters such as power, frequency, polarization, and pulse modulation (or pulse length).

The manuscript is organized as follows. In section II, the four parts of the model are described: the polar F-region, the heat transport phenomena, the pump model, and the method of solution. Section III presents the results in four main parts: the response to HF heating, power dependence, frequency dependence, and effect of HF modulation pulses. A discussion of the results and conclusions are presented in section IV.

II. HF HEATING MODEL

A. Polar F-Region

The model F-region plasma is assumed to be dominated by singly-charged atomic oxygen ions, other ionic species are neglected. The major role of the oxygen ions is to determine the ambipolar rate of expansion of plasma density resulting from HF heating. Of course, these ions also determine the electron-ion collision rate ν_{ei} which is the dominant heating channel in the upper F-region. Prior to irradiation with HF waves, the ionosphere is assumed to be in a state of dynamic equilibrium. The present study is not concerned with determining this equilibrium from basic solar and atmospheric parameters, as is done in purely ionospheric modelling [Schunk and Nagy, 1980], but rather it is assumed that the zero order plasma density and electron temperature profiles are given. The profiles selected for numerical investigation are consistent with those observed experimentally under quiet polar conditions [Bates and Hunsucker, 1974]. The density and temperature profiles selected for discussion in this paper are shown in Figure 1a. The ion temperature T_i is taken to be equal to the neutral temperature T_n. At the lower portion of the F-region the electron temperature drops to the neutral temperature. Throughout the time dependent calculation, both the ion and neutral temperatures are kept constant and equal to each other. This approximation is quite reasonable since the HF predominantly heats electrons, due to their much lighter mass.

It is assumed that the neutrals in the F-region are adequately described by the model of Banks and Kockarts [1973]. The neutral components are: molecular nitrogen (N_2), molecular oxygen (O_2), atomic oxygen (O), atomic hydrogen (H), and helium (He). The altitude concentrations of these neutrals are determined from the Boltzmann factor with a constant temperature $T_n = 750°K$. The resulting neutral density profiles are shown in Figure 1b. From the plas-

ma density and temperature profiles of Figure 1a and the neutral profiles of Figure 1b, one calculates [Banks and Kockarts, 1973] the various momentum transfer collision frequencies entering into the transport description of HF heating, namely, electron-ion collisions ν_{ei}, electron-neutral collisions ν_{en}, and ion-neutral collisions ν_{in}, whose profiles are shown in Figure 1c.

B. Heat Transport

Shortly after the HF pump is turned on, electrons in the F-region begin to heat up due to momentum transfer collisions with neutrals and oxygen ions. The resulting increase in electron temperature is limited by two different mechanisms that operate simultaneously but with varying degree of importance depending on altitude. The two mechanisms are: (1) collisions (due to both elastic and inelastic processes) with neutrals and oxygen ions, and (2) field-aligned electron heat conduction. The role of heat conduction across the magnetic field is relatively unimportant due to the strong electron magnetization in the F-region [Gurevich, 1978], hence it is neglected. Furthermore, heat convection due to bulk plasma drifts across the magnetic field becomes important for time scales of the order of few hundred seconds [Holway et al., 1978]. Since the HF pulse durations considered in this study are shorter than drift times, cross-field heat convection is ignored. Although the neglect of this effect is justifiable in the context of the present study, its role becomes quite important when attempting to describe CW conditions. The reason is that while it usually takes about 10 seconds for the temperature to reach steady state, it takes several minutes for the density to diffuse. Consequently, the plasma drifts away from the HF heated volume before it has time to reach a new pressure equilibrium. The result of this effect invalidates

the density calculations of prior studies based on steady state heating of the F-region [Farley, 1963; Gurevich, 1967; Ignat'ev et al., 1977].

Since electron heat conduction takes place along the magnetic field and the HF pulse considered propagates along $\underline{B}_o$ (for the case $\nabla N_{eo} \times \underline{B}_o = 0$) the transport equations are dominated by field aligned gradients. The weak cross-field gradients arise only through the transverse extent of the HF beam (e.g., the Gaussian cross section of the beam spot). Such weak variations can be treated by considering each field line individually and using the appropriate HF electric field strength on each line. Although this procedure is relatively straightforward to implement, in the present paper we report only on the plasma changes taking place along the field line passing through the center of a Gaussian cross section HF beam. However, the effect of beam divergence is appropriately taken into account in determining the HF electric fields, as derived in part C of this section.

Using a coordinate system in which the z axis points along the direction of increasing height, and the magnetic field of the earth points in the negative z direction (to simulate the northern hemisphere situation), the one-dimensional transport equations that determine the self-consistent evolution of the electron density N_e and temperature T_e take the form

$$\frac{\partial N_e}{\partial t} + \left(\frac{\partial}{\partial z}\hat{\underline{z}}\right) \cdot (N_e \underline{v}_e) = S_o \ , \tag{1}$$

$$N_e \underline{v}_e = \frac{-1}{(m_e \nu_{en} + m_i \nu_{in})} \frac{\partial}{\partial z} [N_e (T_e + T_i)] \hat{\underline{z}} \ , \tag{2}$$

$$\frac{3}{2} k \left[N_e \frac{\partial T_e}{\partial t} + N_e (\underline{v}_e \cdot \hat{\underline{z}}) \frac{\partial T_e}{\partial z}\right] + N_e k T_e \frac{\partial}{\partial z} (\underline{v}_e \cdot \hat{\underline{z}}) = \frac{\partial}{\partial z}\left[K_e \frac{\partial T_e}{\partial z}\right] + Q + Q_o - L_e \ , \tag{3}$$

where k is Boltzmann's constant, $\underline{v}_e$ is the slow electron diffusion velocity, m_e and m_i are the electron and oxygen ion masses, K_e is the parallel coefficient of thermal conductivity, Q is the HF heat source, and L_e represents the rate of electron cooling due to both elastic and inelastic collisions. The terms S_o and Q_o account for the steady state sources that bring about the background equilibrium profiles in the absence of the HF pump. The quantities S_o and Q_o are not calculated explicitly, but rather they can be obtained by setting $\partial/\partial t = 0$ in equations (1) - (3) in which the profiles of Figure 1a are inserted. We assume the origin $z = 0$ at the bottom of the F-region, which is taken to represent an altitude of 150 km.

Equation (2) can be obtained from the electron and ion momentum equations in the appropriate slow time approximation (i.e., neglecting inertia) and for negligible neutral drift velocity. Equation (3) describes the local conservation of electron energy and includes all possible channels for energy gain and loss. The second and third terms on the left hand side of (3) represent the effect of convection and pressure flux, and are found to be negligible in the F-region. However, for completeness they are retained in the numerical calculations.

The quantity describing the rate of electron energy loss $L_e \equiv L_e(z,N_e,T_e,T_i,T_n)$ contains numerous terms not worth reproducing here since they are calculated following the well documented works of Banks and Kockarts [1973], Rees and Roble [1975], and Schunk and Nagy [1980]. However, it is worth emphasizing that L_e includes excitation of rotational and vibrational levels of the molecular species N_2 and O_2, excitation of atomic oxygen fine structure $O(^3P)$ at the ground state, and excitation of atomic oxygen in its first excited state $O(^1D)$. The individual terms contributing to L_e are shown

in Figure 2 for F-region parameters prior to HF heating. The importance of the inelastic processes in the lower F-region is apparent, specially that of the excitation of the $O(^3P)$ level. Electron-ion collisions become the major loss mechanism in the upper F-region.

The coefficient of thermal conductivity used in (3) for a partially-ionized plasma takes the form [Banks and Kockarts, 1973, equation (22.116)]

$$K_e = \frac{7.75\times10^5 T_e^{5/2}}{1+3.22\times10^4 (T_e^2/N_e)\sum_n N_n \langle Q_n \rangle} \text{ eV cm}^{-1} \text{ sec}^{-1} {}^\circ\text{K}^{-1} , \tag{4}$$

where the summation in the denominator is over all the neutral gas species of concentration N_n and average electron-neutral momentum transfer cross section $\langle Q_n \rangle$. The $T_e^{5/2}$ dependence is associated with a fully-ionized plasma and it is modified by the denominator term to account for the effect of the neutral gases.

C. HF Pump

The source term Q appearing in equation (3) is related to the HF electric field amplitude $\underline{E}$ and the high frequency conductivity tensor $\bar{\bar{\sigma}}$ through

$$Q = \langle \mathcal{J} \cdot \mathcal{E} \rangle = \frac{1}{2} \text{Re}[\underline{E}^* \cdot \bar{\bar{\sigma}} \cdot \underline{E}] , \tag{5}$$

where the brackets $\langle\ \rangle$ imply time averaging, $\mathcal{J}$ the total conduction current, and $\mathcal{E}$ the total electric field whose full space-time dependence is given by

$$\mathcal{E}(z,t) = \frac{1}{2}[\underline{E}(z)e^{-i\omega t} + \text{c.c.}] , \tag{6}$$

in which ω is the angular frequency of the HF waves. In general, the total electric field can be described in terms of a right hand circularly polarized component E_+, a left hand circularly polarized component E_-, and a parallel component E_z. In the present geometry ($\nabla N_{eo} \times \underline{B}_o = 0$), and for HF beam propagation along $\underline{B}_o$, only the E_+ and E_- components are relevant. Accordingly, the spatial dependence of the electric field amplitude can be expressed in the form

$$\underline{E}(z) = E_\pm(z) \exp[i \int dz\ \kappa_\pm(z)]\ \hat{\underline{e}}_\pm \ , \tag{7}$$

where

$$\hat{\underline{e}}_\pm = \frac{1}{\sqrt{2}} (\hat{\underline{x}} \pm i\hat{\underline{y}}) \ , \quad \kappa_\pm(z) = k_o \mathcal{N}_\pm(z) \ , \tag{8}$$

where $k_o = \omega/c$, and $\kappa_\pm$ is a complex quantity in general. The local wavenumber $\kappa_\pm(z)$ can itself be positive or negative for either polarization depending on whether the wave is travelling upwards into the ionosphere or downwards after reflection. For the case of principal interest in this study, i.e., overdense heating, both signs of $\kappa_\pm$ must be taken into account. The complex index of refraction $\mathcal{N}_\pm(z) = n_\pm(z) + i\alpha_\pm(z)$, with $n_\pm(z)$ and $\alpha_\pm(z)$ purely real, is related to both the real dielectric and HF electric conductivity by

$$\mathcal{N}_\pm^2(z) = [n_\pm(z) + i\alpha_\pm(z)]^2 = \varepsilon_\pm(z) + i \frac{4\pi}{\omega} \sigma_\pm(z) \ , \tag{9}$$

where $\varepsilon_\pm(z)$ and $\sigma_\pm(z)$ are components of the diagonal dielectric and conductivity tensors, respectively. They are given by

$$\varepsilon_{\pm}(z) = 1 - \frac{(\omega \pm \omega_c)\omega_p^2(z)}{\omega[(\omega \pm \omega_c)^2 + \nu_e^2]} ,$$

$$\sigma_{\pm}(z) = \frac{\nu_e}{4\pi} \frac{\omega_p^2(z)}{[(\omega \pm \omega_c)^2 + \nu_e^2]} , \qquad (10a)$$

the parallel components of these tensors are, respectively,

$$\varepsilon_z(z) = 1 - \frac{\omega_p^2(z)}{(\omega^2 + \nu_e^2)} , \qquad \sigma_z(z) = \frac{\nu_e}{4\pi} \frac{\omega_p^2(z)}{(\omega^2 + \nu_e^2)} , \qquad (10b)$$

where $\omega_p(z)$ is the local electron plasma frequency, ω_c is the electron gyrofrequency, and ν_e is the total electron collision frequency for momentum transfer, i.e., $\nu_e = [\nu_{en}(N_n, T_e) + \nu_{ei}(N_e, T_e)]$. For F-region propagation $\nu_e \ll \omega, \omega_c$, therefore, away from the cut-off layer $\alpha_{\pm}^2(z) \ll n_{\pm}^2(z)$. Accordingly,

$$n_{\pm}(z) \simeq [\varepsilon_{\pm}(z)]^{1/2} , \text{ and } \alpha_{\pm}(z) \simeq \frac{2\pi}{\omega} \frac{\sigma_{\pm}(z)}{n_{\pm}(z)} . \qquad (11)$$

The WKB description of (7), although quite accurate over most of the travel path in the F-region, needs to be corrected for two significant effects: 1) beam divergence due to 3-D propagation; 2) Airy-like behavior near the turning point defined by $\varepsilon_{\pm}(z=z_o) = 0$. The beam divergence correction is introduced by assuming a conical beam spread, as illustrated in Figure 3, and considering the reflection layer to be a perfect mirror of zero width. Conservation of local energy flow requires that

$$\nabla \cdot \underline{P} = - Q(z) , \qquad (12)$$

where $\underline{P}$ is the Poynting vector whose magnitude is P. Integrating (12) over a

volume element having an area equal to the HF beam cross section A(z) yields

$$P(z_2)\,A(z_2) - P(z_1)\,A(z_1) = -\int_{z_1}^{z_2} dz\; A(z)\,Q(z)\;, \tag{13}$$

for two arbitrary heights z_1 and z_2. In reality the beam cross section A(z) corresponds to that of a spherical cap, however in the present context it is approximated by the area of a disk, as is appropriate for narrow beams produced by high gain HF antennas. The ratio of the areas is equal to

$$A(z_1)/A(z_2) = (D + z_1)^2/(D + z_2)^2\;, \tag{14}$$

where D is the distance from the ground-based antenna to the bottom of the F-region at 150 km altitude (z = 0), as indicated in Figure 3. Incorporating the beam divergence effect into equation (7) yields an expression for the electric field which is correct in the region $0 \leq z \leq z_m$, where z_m is a height slightly below the turning point located at z_o as illustrated in Figure 3,

$$E_{\pm}(z) = E(o)[\varepsilon_{\pm}(o)/\varepsilon_{\pm}(z)]^{1/4} \left\{ [A(o)/A(z)]^{1/2} \exp\left[ik_o \int_o^z dz' \mathcal{N}_{\pm}(z')\right] \right.$$
$$\left. + R[A(o)/A(2z_o - z)]^{1/2} \exp\left[-ik_o \int_o^z dz' \mathcal{N}_{\pm}(z')\right] \right\}. \tag{15}$$

Equation (15) contains both an upward travelling wave and a reflected wave with reflection coefficient R. E(o) is the electric field normalized to the HF electric field delivered from a ground-based transmitter to the bottom of the F-region, i.e.,

$$|E(o)| = \left(\frac{2}{1+n_{\pm}(o)}\right)\left(\frac{\sqrt{60\beta WG}}{D}\right) \quad V/m, \tag{16}$$

where W is the average power radiated in watts, G is the antenna gain, D is the distance from the ground in meters, and a simple dipole radiator is assumed. To account for the possibility of HF beam depletion due to absorption in the D and E-regions a factor $0 < \beta \leq 1$ is introduced.

The correction due to Airy-like behavior near the turning point is implemented by having a separate expression for the electric field in the region $z_m \leq z$ given by

$$E_{\pm}(z) = 2\sqrt{\pi}\,(k_o\ell)^{1/6}[\varepsilon_{\pm}(o)]^{1/4}\,E(o)\,[A(o)/A(z)]^{1/2}\,Ai(\zeta - i\Gamma)$$
$$\times \exp\left[ik_o \int_o^{z_o} dz\, \mathcal{N}_{\pm}(z) - i\pi/4\right], \qquad (17)$$

where $\zeta = (k_o\ell)^{2/3}(z-z_o)/\ell$, $\Gamma = (k_o\ell)^{2/3}\,\mathrm{Im}\{\mathcal{N}_{\pm}^2(z)\}$, and it is assumed that near the turning point $\varepsilon_{\pm}(z) = -(z-z_o)/\ell$, where $\ell \equiv [d(\ln N_{eo})/dz]_{z_o}^{-1}$ is the local density scale length at the turning point. The linear density approximation is not a limiting factor in the analysis as long as $(k_o\ell)^{2/3} \gg 1$, i.e., the local ionospheric density scale length (~ 50 km) is much larger than the width of the main lobe of the Airy pattern (~ 500 m). The linear approximation would only be invalidated if the pump frequency and the critical frequency of the F-region are so close, that the cut-off layer and the critical frequency layer are separated by a distance Δz equivalent to the Airy pattern's main width, i.e., $\Delta z \sim \ell/(k_o\ell)^{2/3}$ which is then a case of edge-diffraction not of interest in the present work. However, we should note that in such a case a parabolic density profile at the cut-off layer is a more appropriate choice [Thomson, 1970; Baños and Kelly, 1974].

The asymptotic form of equation (17) matches directly to the WKB solution of equation (15) provided the reflection coefficient R has the form [Budden,

1961]

$$R = -i \exp[-i2k_o \int_o^{z_o} dz \, \mathcal{N}_{\pm}(z)] \, . \tag{18}$$

Thus, we have an analytical description of the HF electric field over the entire F-region. The heat source Q entering in equation (3) can be now simply calculated from equations (5), (10), and (15) or (17).

We should note at this point that in actuality $(k_o \ell)$ is usually so large that $k_o|z_o - z_m| << k_o \ell$, and WKB solutions are valid practically everywhere [Thomson, 1970]. The full wave solution is therefore confined to a small spatial region [Figure 3]. However, within this small region, large amplitude gradients appear and are important in determining the shape and magnitude of the density cavities that are created at the reflection layer.

The total amount of HF power absorption p_a due to Ohmic heating for the overdense case of interest here is given by equation (13) as

$$p_a = \int_o^{z_o} dz \, A(z) < \underline{E}^* \cdot \vec{\sigma} \cdot \underline{E} > = \frac{1}{2} \int_o^{z_o} dz \, A(z) \sigma_{\pm}(z) |E_{\pm}(z)|^2 \, . \tag{19}$$

The F-region absorption coefficient is then defined as

$$\eta \equiv \frac{p_a}{p_{in}} = 1 - |R|^2 \, , \tag{20}$$

where $p_{in} = P(o)A(o)$ is the net HF power input at the bottom of the F-region. Using equation (18) for R results in

$$\eta = 1 - \exp[-4 \int_o^{z_o} dz \, \alpha_{\pm}(z)] \, . \tag{21}$$

According to equation (11), $\alpha_{\pm}(z)$ is a function of both the collision frequencies and the HF frequency. Therefore, the absorption efficiency η is moderately dependent on temperature and density variations via the variation in collision frequencies, but strongly dependent on the variation in HF frequency, as shown in section III C.

D. Method of Solution

The transport equations (1) - (3) together with the scheme for evaluating the heating source Q explained in part C of this section constitute the mathematical formulation of the HF heating model. The mathematical structure consists of a set of coupled nonlinear partial differential equations for the electron density $N_e(z,t)$ and electron temperature $T_e(z,t)$ whose solutions must be obtained numerically. It should be noted that the density equation is highly sensitive to temperature variations, while the equation for the temperature is not strongly affected by the small variations in density.

To formulate a well posed numerical problem a set of boundary conditions must be prescribed at $z = 0$ and at some large value of $z = z_u$, well beyond that corresponding to the critical density of the F-region. At the bottom of the F-region ($z = 0$) we assume that

$$T_e(z=0,t) = T_{eo}(z=0) = T_n \ . \tag{22}$$

This choice is quite reasonable physically, because at the lower heights the electrons are strongly coupled to the neutrals and thus loose their energy quite rapidly. In addition, this choice is consistent with models for D and E-regions heating by HF waves [Tomko, 1981]. It is also assumed that at the lower boundary

$$N_e(z=0,t) = N_{eo}(z=0) \ . \tag{23}$$

This condition is justified because the density changes produced by HF heating are maximized near the reflection layer ($z = z_o$) and even there they tend to be small (of the order of few percent, as is shown in section III A).

At the upper boundary $z = z_u$ we demand that the gradients of the zero-order profiles remain unchanged, i.e.,

$$\left[\frac{\partial}{\partial z} T_e(z,t)\right]_{z_u} = \left[\frac{\partial}{\partial z} T_{eo}(z)\right]_{z_u} \ ,$$

$$\left[\frac{\partial}{\partial z} N_e(z,t)\right]_{z_u} = \left[\frac{\partial}{\partial z} N_{eo}(z)\right]_{z_u} \ . \tag{24}$$

This choice is motivated by the physical idea that the particle and heat fluxes at altitudes between 800 km to 1000 km are not likely to be influenced by HF pulses that reflect around 250-300 km altitudes. However, from a rigorous point of view the upper boundary conditions are unknown since the plasma there tends to be collisionless, hence it does not admit a fluid transport description. In practice, the upper boundary introduces numerical reflections which can invalidate some results, in particular, the density changes produced by long HF pulses. However, all the results reported in the present work are obtained in the regime where the sensitivity to the upper boundary is negligible.

Equations (1)-(3) are solved using a predictor-corrector form of the time averaged Crank-Nicholson tridiagonal method [Douglas and Jones, 1963]. The spatial grid scale is chosen so that it resolves heights as small as 250 m, while the smallest time scales resolvable are of the order of 100 ms. Non-

linear coefficients are updated to half the time step before the variables are time averaged over a full time step. The new values of density and temperature are then fed back into all the dependent parameters of the analysis. Specifically, the feedback of the heating on the source term Q shows through the collision dependent parameters, i.e., the conductivity $\sigma_{\pm}$ and the absorption $\alpha_{\pm}$. The effect of the density variation on the spatial shape of the HF field near the reflection layer is neglected because the density changes are small. Also, in our computations we average the spatial sinusoidal variations resulting from the interaction between the incident and reflected waves, the reason being that their scale length is usually smaller than the collision length of the particles, making the transport analysis insensitive to their effect. However, this approximation does not affect the magnitude and shape of the large main Airy pattern lobe, especially on the evanescent high density side, which is important in calculating the density modification.

III. NUMERICAL RESULTS

A. Response to HF Heating

The HF transmitter characteristics chosen in the numerical study of equations (1)-(3) correspond roughly to those available at the experimental facilities in Norway and Alaska. The HF frequency is taken as $\omega/2\pi = 5.1$ MHz, a radiated power of W = 1 MW is chosen, and an antenna gain G = 20 dB is assumed. A pure left hand circularly polarized wave (corresponding to x-mode for oblique case) is considered in this geometry ($\nabla N_{eo} \times \underline{B}_o = 0$). The results obtained with this heating mode are easily extrapolated to the case of a finite, but small, angle between ∇N_{eo} and $\underline{B}_o$, as the characteristics of the left hand wave (x-mode) change slowly with small angular variations. The right hand circularly polarized mode (corresponding to o-mode for oblique case) which reflects at a higher altitude, has similar Ohmic absorption characteristics to the left hand mode; however, the results obtained for a purely longitudinal geometry cannot be extrapolated to the case of a finite angle between ∇N_{eo} and $\underline{B}_o$. For such a polarization one must properly include the effect of electrostatic modes appearing near the layer where $\omega_p(z) = \omega$ [Meltz et al., 1974], as well as the effect of Z-trace propagation, both of which create new absorption channels in addition to Ohmic heating. The D and E-regions transmission factor β is arbitrarily taken as $\beta = 0.75$, which corresponds to weak D and E-region conditions, a situation consistent with the quiet F-region profiles shown in Figure 1a.

We proceed next to describe the results obtained from heating with typical HF pulses 90 seconds long. The relaxation of the F-region is observed for 60 seconds after the HF pulse is turned off.

The altitude dependence of the local Ohmic heating absorption rate

$Q = (\sigma_-|E_-|^2)/2$, obtained from equation (5), is shown in Figure 4a. In the neighborhood of z = 150 km, the absorption is reduced due to two effects: 1) beam divergence and consequent $[1/(D+z)^2]$ decrease in $|E_-|^2$; 2) wave attenuation due to electron collisions (which decrease with altitude). A sharp increase in Q exists at the reflection layer as $\varepsilon_-(z) \to 0$ because of the $|\varepsilon_-(z)|^{-1/2}$ dependence of $|E_-|^2$; the maximum amplitude, however, is correctly limited by the Airy function as given in equation (17).

Figure 4b shows the altitude dependence of the fractional change in electron temperature, normalized to the local pre-heating temperature $T_{eo}(z)$, for different times in the evolution. The HF pulse is turned on at t = 0. For early times, t < 1 s (not shown), the spatial variation of the temperature is essentially the same as that of the HF power, i.e., the process is local and is thus maximized around the reflection layer. Electron thermal conduction rapidly (within 1 s) starts diffusing heat from regions of high concentration near the reflection layer and at the bottom boundary to cooler regions along the magnetic field lines (t = 3 s). The temperature profile broadens consequently from the bottom of the F-region (z = 0, at 150 km) to the reflection layer ($z = z_o$, at 206 km), with a small foot expanding beyond the reflection layer to the region of higher thermal conductivity (t = 15 s). Equilibrium is attained between z = 0 and z_o essentially within 10 seconds (equilibrium time being defined as the time for the variation to reach over 95% of its value), and a maximum local change of about 50% is produced. After 90 s, the temperature of the whole F-region is well into the steady state equilibrium regime. After the HF pulse is turned off, thermal conduction relaxes the temperature profile between z = 0 and z_o essentially back to its unperturbed level within 10 seconds (t = 105 s). One minute after the heating is turned off, at t = 150 s, there is almost no trace of HF heating in the electron temperature.

The relatively fast relaxation of the temperature is to be contrasted with the behavior of the density modification, which responds on a much longer time scale because it is regulated by ambipolar diffusion. The density changes are triggered by local increases in plasma pressure resulting from the temperature increases. Specifically, the rate of density change is governed by the second spatial derivative of the electron temperature. Consequently, for early times after turning on the HF pulse, the density profile experiences an impulse-like driving force having a spatial dependence sharply peaked at the reflection layer (on the higher density side). This effect produces a dent in the density profile as seen in Figure 4c. This figure illustrates the time evolution of the fractional density change, normalized to the local unperturbed value $N_{eo}(z)$, and it shows the slow development of a "thermal caviton" having a spatial scale initially determined by the width of the electromagnetic Airy pattern. This density cavity is to be distinguished from other analogous effects previously discussed in the plasma physics literature, e.g., ponderomotive density cavities which can be generated at short scales by electrostatic waves, or at long scale lengths by standing electromagnetic waves. Actually, it can be shown that the ratio of the ponderomotive force produced by the Airy pattern of (17) to the kinetic pressure force producing these thermal cavitons is of the order of (m_e/m_i). As seen in Figure 4c, the growth of the density cavity continues throughout the length of the HF pulse; eventually the cavity attains a depth of about 2% of the unperturbed density and extends over a length of ~10 km. One minute after turning off the HF, at $t = 150$ s, the cavity still exists near the cut-off layer at a level $|\delta N/N_{eo}| \sim 1\%$. The diffusion velocity is so small [equation (2)] that the cavity is almost static during the short time of the experiment.

A closer examination of Figure 4c reveals another density cavity located at a height slightly above the lower numerical boundary. Although the depth of this lower cavity is indeed enhanced by our choice of a rather abrupt cooling of the electron temperature at the lower end, the qualitative existence of such a cavity is expected on first principles. This second cavity arises because a second order spatial derivative in temperature must develop in the transition from E-region to the lower F-region, hence an effect analogous to the impulsive drive encountered at the HF cut-off must also occur at a lower height. A density "bump" is created between the two cavities. It attains a level $\delta N/N_{eo}$ of the order of 0.5% after 90 s of heating and relaxes at a rate much slower than the cavities.

Figure 4d shows the electron-neutral and electron-ion cooling losses before HF heating (t = 0), after HF heating is on (t = 90 s), and one minute after HF heating is turned off (t = 150 s). It is interesting to note the large temperature dependence of the inelastic electron-neutral cooling processes. Their presence plays an important role in limiting the heating of the electrons. This effect, together with thermal conduction, limits the production of the thermal runaway process discussed by Perkins and Roble [1978].

Figure 4e shows the behavior of the transverse d.c. Pedersen electrical conductivity $\sigma_p(z,T_e)$ and the parallel d.c. electrical conductivity $\sigma_\parallel(z,T_e)$ for the electrons before HF heating (t = 0), after heating is on (t = 90 s), and one minute after it is turned off (t = 150 s). We do not show the Hall conductivity because it is not sensitive to temperature changes, and remains essentially constant in the F-region because the density changes are small. Equations (10) show that when $\omega = 0$ (d.c. case), $\sigma_p \propto \nu_e$ and $\sigma_\parallel \propto \nu_e^{-1}$, yielding

$$|\delta\sigma_\parallel(z,T_e)/\sigma_{\parallel o}(z)| \simeq \frac{\nu_{eo}(z)}{\nu_e(z,T_e)} |\delta\sigma_p(z,T_e)/\sigma_{po}(z)| , \qquad (25)$$

where $\sigma_{po}(z)$, $\sigma_{\parallel o}(z)$, $\nu_{eo}(z)$ are the initial values before heating. Heating decreases ν_e in the middle and upper F-region where electron-ion collisions are dominant. It increases ν_e in the lower F-region where electron-nitrogen momentum transfer collisions are dominant. This behavior is observable in the variation of σ_p and $\sigma_\parallel$ in Figure 4e. It is of interest to estimate the total change in the electrical resistance along a magnetic flux tube of fixed cross section in the F-region. Alternatively, the variation in the height-integrated parallel resistivity is given by:

$$\frac{\Delta r_\parallel}{r_{\parallel o}} = \int_o^{z_u} \left[\frac{1}{\sigma_\parallel(z,T_e)} - \frac{1}{\sigma_{\parallel o}(z)} \right] dz \Big/ \int_o^{z_u} \frac{dz}{\sigma_{\parallel o}(z)} , \tag{26}$$

where $r_\parallel$ is the parallel resistance of the flux tube and $r_{\parallel o}$ is its value before heating (the effect of the ions being negligible). We find that after 90 s of heating, the parallel resistance in the F-region has decreased by about 4%. The corresponding variation in the height integrated Pedersen resistivity is negligible as it is dominated by the unchanged ion component. The net effect may alter the flow of naturally occuring auroral currents (Birkland currents) by favoring their parallel flow in the F-region and lowering the altitude of their return path at the E-region heights. Such interactions are of physical interest and warrant further study.

A common feature in the results shown in Figure 4 is that maximal variation occurs near the reflection layer, where maximum Ohmic absorption takes place. In Figure 5 we show the time variation at the reflection layer z_o (corresponding to an altitude of 206 km) of the temperature, the density, and the electron Pedersen conductivity, respectively. The rapid rise and decay time of the temperature, as previously mentioned, is more visible in Figure 5a and is found to possess an e-folding time of about 1 s. The slow diffusio of

the density is shown in Figure 5b. Contrary to the temperature, no steady state or return to background conditions is observed, only slow rise and decay. The variation of the electron Pedersen conductivity follows closely that of the temperature as seen in Figure 5c. The long term steady state is altered only by the very small, continuous variation of the density. The corresponding variation of the parallel conductivity can be inferred from Equation (25), whence it is expected to look similar to that of the Pedersen component, but positive in magnitude.

B. Power Dependence

The numerical results discussed thus far correspond to the effects produced by a fixed average radiated power W = 1 MW. Due to the nonlinear dependence of the various collisional processes on electron temperature, the resulting values of the temperature variation, depth of density cavities, and other dependent parameters are, in general, nonlinear functions of the radiated power. To study such nonlinear behavior we proceed to vary the radiated power with parameters similar to those used in section III A, specifically a fixed frequency of 5.1 MHz and a pulse length of 90 s. The time evolution of the temperature and density at the reflection layer z_o (corresponding to an altitude of 206 km) are shown in Figure 6, and the dependence of these variations on the radiated power, after 90 s of heating, is shown in Figure 7. The variation of the electron Pedersen conductivity is also shown in Figure 7 (curve c). Besides the larger variations achieved with higher power, Figure 6 also shows that the rise and decay equilibrium times for the temperature are power dependent, the higher the power the shorter the time (~10 s for W = 1 MW, and ~5 s for W = 5 MW). This effect is stronger as one moves toward lower F-region altitudes (not shown). It is seen from Figure 7 that clear departure

from linearity sets in at powers larger than W = 1 MW. Saturation of both the temperature and the conductivity (curves a and c) seem to be attainable at power levels higher than W = 10 MW. Curve b shows that density cavities with depths of about 4% of the background density may be attained at power levels $W \gtrsim 5$ MW.

The spatial variation of the electron temperature for different power levels is shown in Figure 8 where it is seen that temperature variations over 120% are attained in the lower F-region for $W \gtrsim 5$ MW. Also, heat conduction for $W \gtrsim 5$ MW can increase the temperature of the upper F-region by almost 10% of its background value.

C. Frequency Dependence

The next variation we investigate is the dependence of the ionospheric modifications on the choice of HF frequency for fixed average radiated power W = 1 MW, and with other parameters similar to those used in section III A. All cases presented correspond to overdense heating (where $\omega < \omega F_{2max}$). Furthermore, to illustrate the degree of variability which may be encountered in field experiments, we consider two model ionospheres having identical height dependence (self-similar profiles), but with different critical frequencies ωF_{2max}. The first model, a (shown in Figure 1a), has $N_{eo}(0) = 5 \times 10^4 cm^{-3}$, and the second model, b, has $N_{eo}(0) = 10^5 cm^{-3}$.

Figure 9 shows the dependence of the F-region absorption coefficient η on HF frequency for the two model ionospheres a and b. The solid curves correspond to conditions prior to application of the HF pulse while the dashed curves represent the situation after 90 s of HF heating. The noticeable dependence in Figure 9 is the increase of the absorption with HF frequency, a result associated with the longer absorption path length travelled by the higher

frequency pulses. Depending on the frequency and the density profile, the absorption coefficient η varies between 20-60% for the quiet conditions of our model. For neutral temperatures corresponding to higher solar activity the upper bound on η may be over 80%. Another dependence seen in Figure 9 is that after 90 s of heating the absorption coefficient drops by about 5-10% from its initial value. This behavior is to be contrasted with that occuring for frequencies that reflect near the lower F-region where the absorption increases after the application of the HF, a characteristic of the D and E-regions.

The relative variation of the temperature produced at the reflection layer after 90 s of HF heating (steady state) is plotted against frequency in Figure 10 for the two model ionospheres a and b. The behavior is characterized by temperature increases between 50-90% at lower frequencies, which correspond to reflection in the highly collisional lower F-region. The temperature variation decreases as the HF frequency increases and reaches a nearly constant value of $[\delta T_e/T_{eo}(z)] \sim 30\%$, for both ionospheres a and b. This flattening effect arises for HF frequencies which reflect in the region located below the F-region peak where the total electron collision frequency ($\nu_e = \nu_{ei} + \nu_{en}$) exhibits a weak spatial dependence.

Figure 11 shows the frequency dependence of the peak relative change in density associated with the cavities generated at the reflection layer after 90 s of heating. The overall dependence of the density cavity follows essentially the same behavior exhibited by the temperature as expected, since their formation is triggered by the sharp temperature gradients at the reflection layer. An additional feature is observed in Figure 11. Instead of approaching a flat frequency dependence at the higher frequencies as in Figure 10, the magnitude of $[\delta N_e/N_{eo}(z)]$ tends to increase. This secondary effect is associ-

ated with frequencies that reflect at higher altitudes where the exponentially decreasing ion-neutral collision frequency is responsible for increasing the rate of ambipolar expansion.

Finally, a general observation regarding the previous results. The curves in Figures 9, 10, and 11 for ionosphere b are almost similar to those obtained for ionosphere a but shifted towards higher frequencies. This is an indication that the depth of penetration inside the F-region, rather than the frequency itself, is the major factor in determining the magnitude of the variation of the parameters.

D. HF Modulation Pulses

The effect of modulating the F-region with HF pulses repeated at low frequency (ULF range) is a topic of general interest which we investigate here using a 1 Hz square amplitude modulation of the HF pump. All HF parameters are similar to those used in section III A, specifically, the frequency is set at 5.1 MHz and the average radiated power is initially assumed to be W = 1 MW. Figure 12a shows the modulation of the electron temperature and Figure 12b the corresponding modulation of the electron Pedersen conductivity, from which the modulation of the parallel conductivity can also be inferred using equation (25). With the power held at W = 1 MW we modulate from steady state conditions after 30 s of HF heating. We obtain about 2.5% modulation of the conductivity corresponding to 5% modulation of the temperature. If we reduce the pre-modulation heating time to 5 s keeping W = 1 MW and then modulate at 1 Hz (i.e., we do not modulate from steady state), the result is the same. If we double the power to W = 2 MW, again with 5 seconds heating before the 1 Hz modulation, we notice that the initial variation of both the temperature and conductivity is larger, however the conductivity modulation attained is only

augmented to approximately 3% corresponding to about 9% temperature variation. The modulations are evaluated at the reflection layer of the HF wave, hence they correspond to maximal variation as is shown in section III A. It is suggestive then that in order to enhance the modulation of the conductivity one should use a pump frequency that reflects in the lower F-region where higher electron collision rates prevail. This idea, however, is only partially correct. As may be seen from Figure 4e, there is a location in the F-region where the Pedersen conductivity increases ($\sigma_\parallel$ decreases) with temperature instead of decreasing ($\sigma_\parallel$ increasing) as is the case in the rest of the F-region. This behavior is related to changing from a domain where electron-nitrogen collisions dominate to one where electron-ion collisions dominate. Therefore, there exists a layer in the lower F-region, between 160-200 km altitude for the present case, where both effects tend to cancel each other and in the neighborhood of which large temperature variations produce no significant modulation of the conductivity.

The effect of the modulation on the density is to keep the depth of the density cavities nearly constant, i.e., at the level attained just before modulation starts.

IV CONCLUSIONS

We have presented a model for the Ohmic heating by HF waves of the polar ionosphere F-region. The geometry of this high-latitude allows a self-consistent analysis of overdense heating. The ability to analytically model the spatial behavior of the HF electric field proves essential in obtaining accurate estimates of the changes produced in the temperature and density profiles.

Ohmic absorption varying from 20% to 80% is attainable, depending mainly on the HF frequency and solar activity cycle. Maximum ionospheric modification is found to occur near the reflection layer where Ohmic absorption is largest. This behavior is in agreement with experimental data [e.g., Gordon and Carlson, 1974], and results in the formation of localized thermal cavitons. Maximum electron temperature increases in the range of 20-120% are obtained for HF power levels ranging between 0.2-5 MW, and exhibit a fast rise and decay equilibrium time of 7-10 s (depending on altitude) for powers near $W \sim 1$ MW, and of 2-5 s (depending on altitude) for higher powers $W \gtrsim 5$ MW. These times are shorter than those for mid-latitude heating, however the general behavior is consistent with experimental observations [e.g., Gordon and Carlson, 1974; Mantas, et al., 1981] as well as with previous calculated values [Meltz and Lelevier, 1970].

The thermal density cavities produced at the reflection layer are a few kilometers in extent along the earth's magnetic field and, depending on HF power and pulse length, can attain a depth of 1-10% of the local background density. These values agree with the density changes inferred from experiments [e.g., Minkoff, 1974; Duncan and Behnke, 1978]. The response time of these termal cavitons is slow, of the order of minutes. Hence they remain

for a considerable time after the HF pulse is turned off. This behavior results in a memory-type effect, whereby in a repeated HF pulse scenario with off time of seconds to few minutes, the ionosphere "remembers" the effect of previous pulses. Any pre-existing density cavity, whether produced by a previous HF pulse or naturally occurring, can be stimulated into growing by subsequent HF pulses. For instance, the depth of the density cavity formed with 1 Hz modulation presented in section III D can be maintained at essentially a constant level. The existence of such cavities near the reflection layer can in turn modify the reflection properties of test signals, such as ionosondes. Such an effect is consistent with the experimental observation, first seen in Platteville, of artificial spread-F persisting long after the HF pump has been turned-off [Utlaut and Violette, 1974].

The present study strongly suggests that the large estimates of density modification calculated from steady state analysis of the temperature, via the pressure equilibrium condition, are never reached in practice [e.g., Farley, 1963; Gurevich, 1967; Ignat'ev et al., 1977]. The reason is that it takes several minutes for pressure equilibrium to be attained. However, on these time scales plasma drifts would shift the heated volume out of the HF beam cross-section [Holway et al., 1978], thus limiting the maximum value of the density changes produced. The present study tends to show a general agreement with the estimates of the time dependent analysis of Meltz and Lelevier [1970] and Meltz, Holway, and Tomljanovich [1974] which are obtained for a mid-latitude ionospheric model.

It has also been found in the present study that HF pulses can change the d.c. electrical resistance along a magnetic flux tube, decreasing it by about 4%.

This suggests the possibility that parallel auroral Birkland currents may be modified with HF heating by forcing their return path towards lower altitudes.

Finally, a useful result can be inferred from the study reported here for ionospheric F-region experiments that aim to investigate F-region wave-plasma phenomena such as wave beating [Shoucri et al., 1982], parametric decay instabilities [Perkins et al., 1974], electrostatic plasma line effects [Gordon and Carlson, 1974], etc. Such experiments use characteristic pulse lengths of the order of a few msec to a few hundred msec. According to the present results such time scales are extremely short compared to the longer time scales for Ohmic heating, cooling, and density diffusing. Consequently, the HF pump is expected to have a negligible effect on the background ionosphere during such short time experiments. However, the use of repetitive pulses at small time intervals to conduct such experiments as well as the use of pulse lengths of a few seconds can produce significant changes in the background ionosphere.

ACKNOWLEDGMENT: This work has been supported by the Office of Naval Research.

REFERENCES

Banks, P. M., and G. Kockarts, Aeronomy A and B, Chs. 1, 9 and 22, Academic Press, New York, 1973.

Baños, A., and D. L. Kelly, Electromagnetic wavefunctions for parabolic plasma density profiles, Phys. Fluids, 17, 2275, 1974.

Bates, H. F., and R. D. Hunsucker, Quiet and disturbed electron density profiles in the auroral zone ionosphere, Radio Sci., 9, 455, 1974.

Budden, K. G., Radio Waves in the Ionosphere, Ch. 16, Cambridge University Press, London, England, 1961.

Douglas, J., and B. F. Jones, On predictor-corrector methods for nonlinear parabolic differential equations, J. SIAM. 11, 195, 1963.

Duncan, L. M., and R. A. Behnke, Observations of self-focusing electromagnetic waves in the ionosphere, Phys. Rev. Lett., 41, 998, 1978.

Farley, D. T., Artificial heating of the electrons in the F-region of the ionosphere, J. of Geophys. Res., 68, 401, 1963.

Gordon, W. E., and H. C. Carlson, Arecibo heating experiments, Radio Sci., 9, 1041, 1974.

Gurevich, A. V., Effect of radio waves on the ionosphere in the vicinity of the F-layer, Geomagn. Aeron., 7, 291, 1967.

Gurevich, A. V., Nonlinear Phenomena in the Ionosphere, Ch. 5, Springer-Verlag, New York, 1978.

Holway, L. H., A. H. Katz, and G. Meltz, Ionospheric effects of a high power space-borne microwave beam, in Effect of the Ionosphere on Space and Terrestrial Systems, edited by J. M. Goodman, p. 354, U.S. Govt. Printing Office, Washington, D.C., 1978.

Ignat'ev, Yu. A., Z. N. Krotova, and E. E. Mityakova, Calculation of the electron density of the F-region heated by a high power radio-wave field,

Radiofiz., 20, 1267, 1977.

Mantas, G. P., H. C. Carlson, and C. H. LaHoz, Thermal Response of the F-region ionosphere in artificial modification experiments by HF radio waves, J. Geophys. Res., 86, 561, 1981.

Meltz, G., and R. E. LeLevier, Heating the F-region by deviative absorption of radio waves, J. Geophys. Res., 75, 6406, 1970.

Meltz, G., L. H. Holway, and N. M. Tomljanovich, Ionospheric heating by powerful radio waves, Radio Sci., 9, 1049, 1974.

Minkoff, J., Radio frequency scattering from a heated ionospheric volume, 3, Cross section calculations, Radio Sci., 9, 997, 1974.

Perkins, F. W., C. Oberman, and E. J. Valeo, Parametric instabilities and ionospheric modification, J. Geophys. Res., 79, 1478, 1974.

Perkins, F. W., and R. G. Roble, Ionospheric heating by radio waves: Predictions for Arecibo and the satellite power station, J. Geophys. Res., 83, 1611, 1978.

Rees, M. H., and R. G. Roble, Observations and theory of the formation of stable auroral red arcs, Rev. of Geophys. and Space Phys., 13, 201, 1975.

Shoucri, M., G. J. Morales, and J. E. Maggs, Beat excitation of whistler waves, Phys. Fluids, 25, 1824, 1982.

Schunk, R. W., and A. F. Nagy, Ionosphere of the terrestrial planets, Rev. of Geophys. and Space Phys., 18, 813, 1980.

Stubbe, P., H. Kopka, H. Lauche, M. T. Rietveld, A. Brekke, O. Holt, T. B. Jones, T. Robinson, A. Hedberg, B. Thidé, M. Crochet, and H. J. Lotz, Ionospheric modification experiments in northern Scandinavia, J. Atmos. Terr. Phys., 44, 1025, 1982.

Thomson, J. A., Energy deposition in artificial ionospheric heating experiments, J. Geophys. Res., 75, 6446, 1970.

Tomko, A. A., Nonlinear phenomena arising from radio wave heating of the lower ionosphere, Report PSU-IRL-SCI-470, Ionosphere Research Laboratory, Pennsylvania State University, University Park, Pennsylvania, 1981.

Utlaut, W. F., and E. J. Violette, A summary of vertical incidence radio observations of ionospheric modification, Radio Sci., 9, 895, 1974.

Wong, A. Y., J. Santoru, and G. G. Sivjee, Active stimulation of the auroral plasma, J. Geophys. Res., 86, 7718, 1981.

FIGURE CAPTIONS

Figure 1 The ionospheric F-region model: a) zero order Chapman electron density and temperature profiles; b) density profiles of various neutral components; c) elastic momentum transfer collision profiles.

Figure 2 Different electron cooling mechanisms in the F-region evaluated at equilibrium prior to HF heating and due to: elastic collisions between electron-neutrals $(e\text{-}n)^{EL}$ and electron-ions e-i; inelastic collisions between electrons and rotational levels $e\text{-}N_2^R$ and $e\text{-}O_2^R$, vibrational levels $e\text{-}N_2^V$ and $e\text{-}O_2^V$, oxygen fine structure of ground level $e\text{-}O\,^3P$, and oxygen first excited state $e\text{-}O\,^1D$; e-n is the total electron-neutral losses.

Figure 3 Schematic diagram for the HF heating of the polar F-region. The distribution of the squared HF electric field is shown, and its fine structure near the reflection layer is magnified in the boxed area.

Figure 4 Ionospheric response to a 5.1 MHz, left handed circularly polarized (L- or x-mode) HF pulse of length t = 90 s; radiated power W = 1 MW, antenna gain G = 20 dB, D and E-regions transmission factor $\beta = 0.75$, after-pulse cooling time 60 s. Shown is the altitude dependence at different times of: a) Ohmic heating $Q = \sigma_- |E_-|^2/2$; b) electron temperature variation, $\delta T_e = T_e(z,t) - T_{eo}(z)$; c) plasma density variation, $\delta N_e = N_e(z,t) - N_{eo}(z)$; d) electron cooling losses due to neutrals L_{en} and ions L_{ei}; e) variation of the electron Pedersen and parallel conductivities, σ_p and $\sigma_\parallel$ respectively.

Figure 5 Time variation at the reflection layer ($z_o \equiv 206$ km, measured from the ground) of: a) electron temperature; b) plasma density; c) electron Pedersen Conductivity. Same HF pump parameters as in Figure 4.

Figure 6 Time variation at the reflection layer ($z_o \equiv 206$ km, measured from the ground) of: a) electron temperature, and b) plasma density, for different HF radiated powers W = 0.2, 1, and 5 MW. Other HF pump parameters are similar to Figure 4.

Figure 7 Power dependence at the reflection layer ($z_o \equiv 206$ km, measured from the ground) of the electron temperature, plasma density, and electron Pedersen conductivity for the HF pump parameters of Figure 4.

Figure 8 Spatial changes of the electron temperature for different HF power levels.

Figure 9 Frequency dependence of the Ohmic absorption coefficient η before (t = 0) and after heating (t = 90 s) for two self-similar density profiles having: (a) $N_{eo}(0) = 5 \times 10^4$ cm^{-3}, and (b) $N_{eo}(0) = 10^5$cm^{-3}; W = 1 MW, G = 20 dB, L- or X-mode.

Figure 10 Dependence of the electron temperature changes at the reflection height on frequency, after 90 s of heating. Results are shown for two self-similar density profiles having (a) $N_{eo}(o) = 5 \times 10^4$cm^{-3}, and (b) $N_{eo}(o) = 10^5$cm^{-3}; W = 1 MW, G = 20 dB, L-mode, $\beta = 0.75$. Temperature values are normalized by the pre-heating temperature at the respective reflection heights.

Figure 11 Dependence of the plasma density changes at the reflection height on frequency, after 90 s of heating. Results are shown for two self-similar density profiles having (a) $N_{eo}(0) = 5 \times 10^4$cm^{-3}, and (b) $N_{eo}(0) = 10^5$cm^{-3}; W = 1 MW, G = 20 dB, L-mode, $\beta = 0.75$. Density values are normalized by the pre-heating densities at the respective reflection heights.

Figure 12 Electron temperature (a) and conductivity (b) modulation by a 1 Hz pulsed HF wave after 30 s of heating at W = 1 MW, after 5 s of heating at W = 1 MW, and after 5 s of heating at W = 2 MW; f = 5.1 MHz, G = 20 dB, L-mode. Values calculated at the reflection layer ($z_o \equiv 206$ km, measured from the ground). Note the change in time scale.

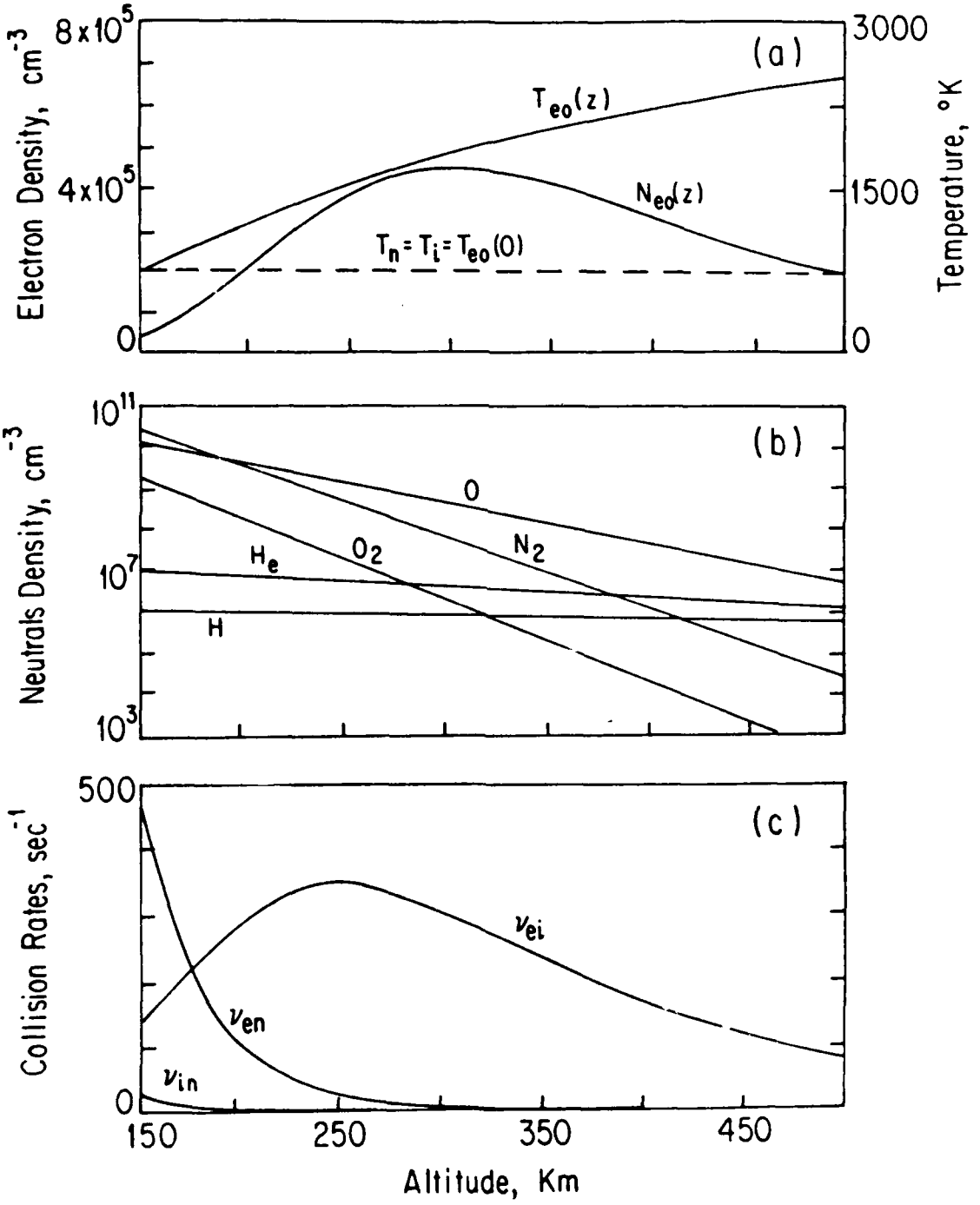
(a)
8×10^5
4×10^5
0
Electron Density, cm^{-3}
3000
1500
0
Temperature, °K
$T_{eo}(z)$
$N_{eo}(z)$
$T_n = T_i = T_{eo}(0)$
(b)
10^{11}
10^7
10^3
Neutrals Density, cm^{-3}
O
N_2
O_2
H_e
H
(c)
500
0
Collision Rates, sec^{-1}
ν_{ei}
ν_{en}
ν_{in}
150
250
350
450
Altitude, Km

Fig. 1

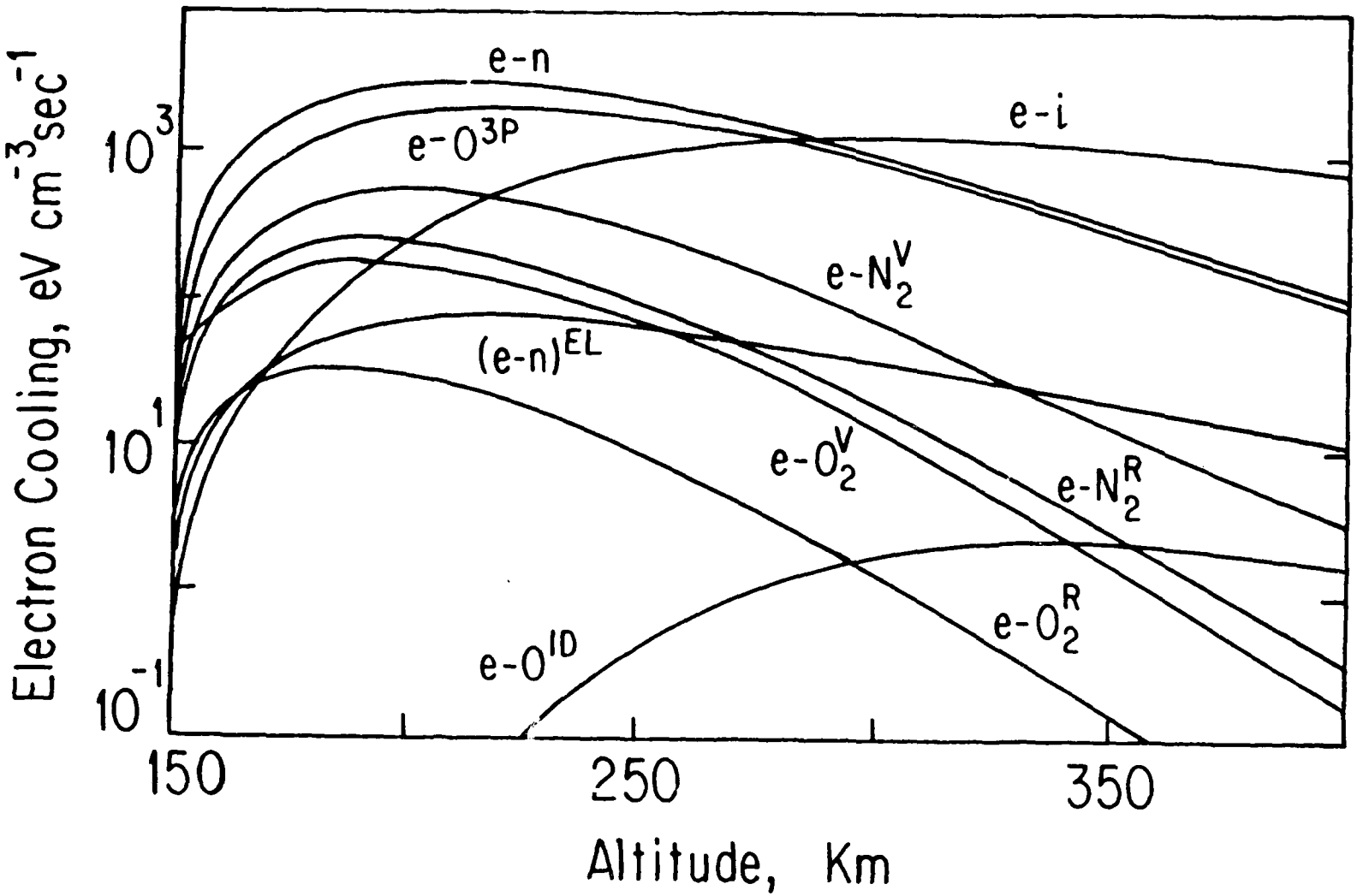
Electron Cooling, eV cm^{-3}sec^{-1}
10^3
10^1
10^{-1}
e-n
e-O^{3P}
e-i
e-N_2^V
(e-n)^{EL}
e-O_2^V
e-N_2^R
e-O_2^R
e-O^{1D}
150
250
350
Altitude, Km

Fig. 2

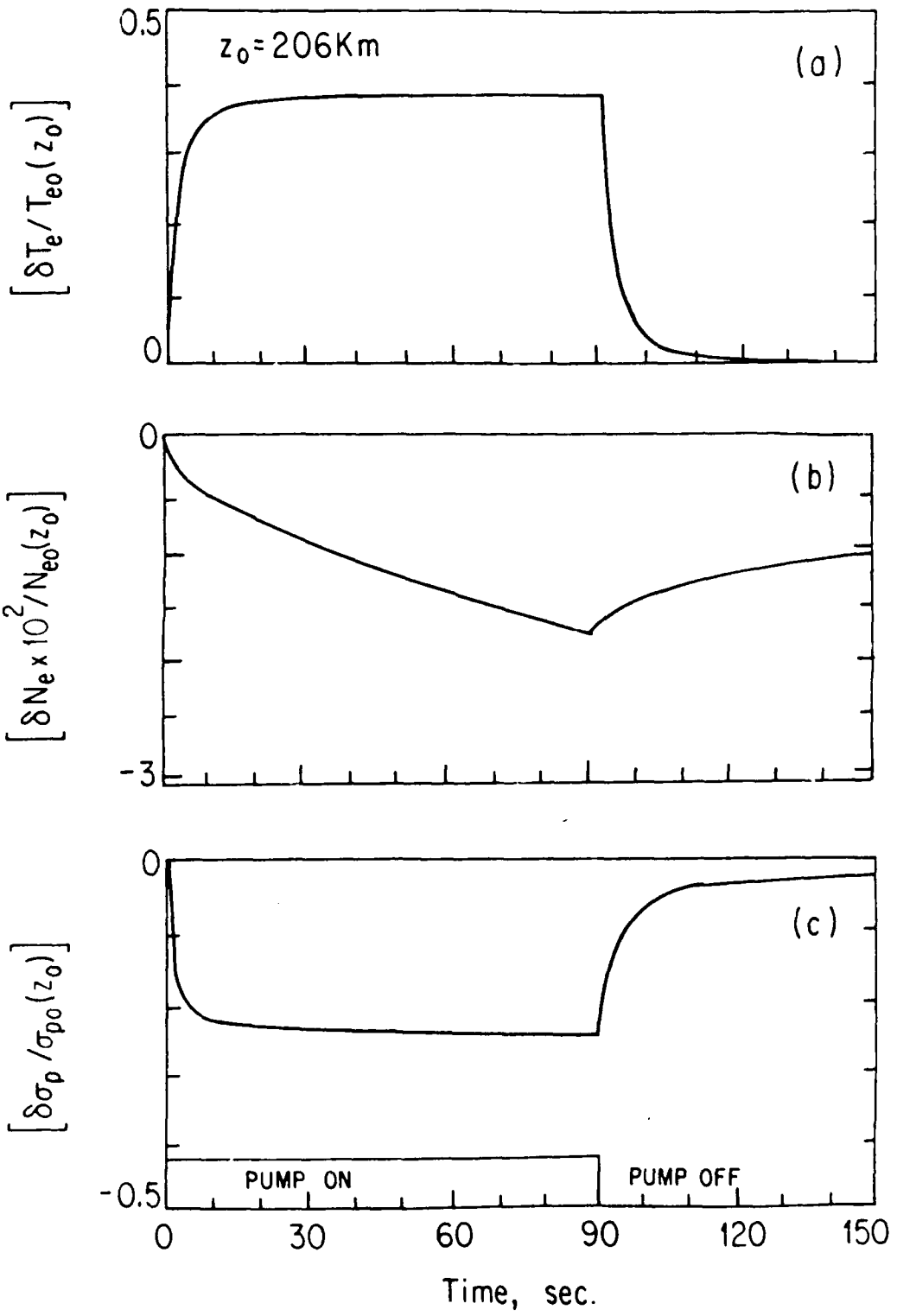
0.5
$z_0 \simeq 206$Km
(a)
$[\delta T_e / T_{eo}(z_0)]$
0
0
(b)
$[\delta N_e \times 10^2 / N_{eo}(z_0)]$
-3
0
(c)
$[\delta \sigma_p / \sigma_{po}(z_0)]$
-0.5
PUMP ON
PUMP OFF
0
30
60
90
120
150
Time, sec.

Fig. 5

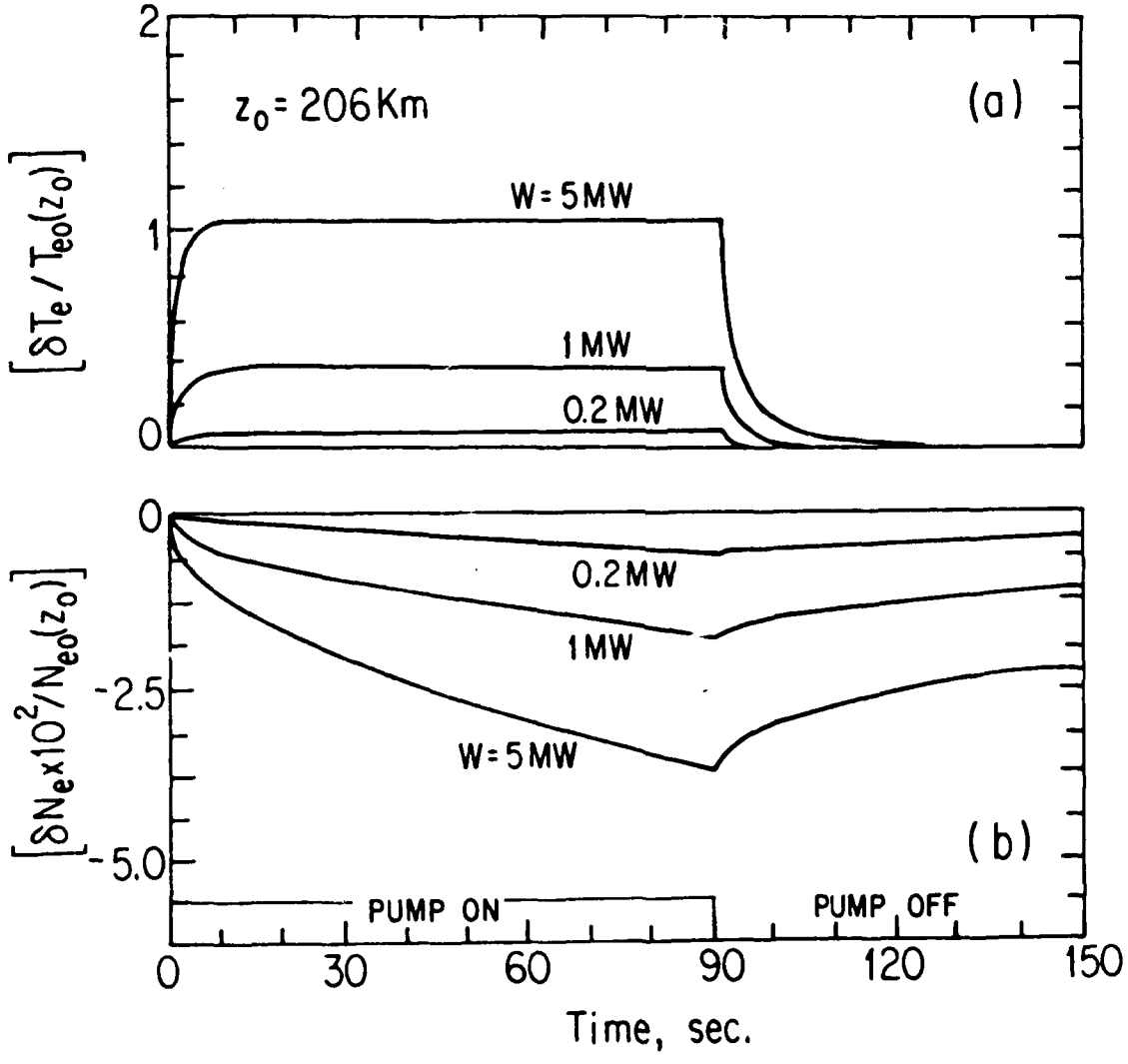
2
1
0
z_0 = 206 Km
(a)
W = 5MW
1MW
0.2MW
$[\delta T_e / T_{eo}(z_0)]$
0
-2.5
-5.0
0.2MW
1MW
W = 5MW
(b)
$[\delta N_e x 10^2 / N_{eo}(z_0)]$
PUMP ON
PUMP OFF
0
30
60
90
120
150
Time, sec.

Fig. 6

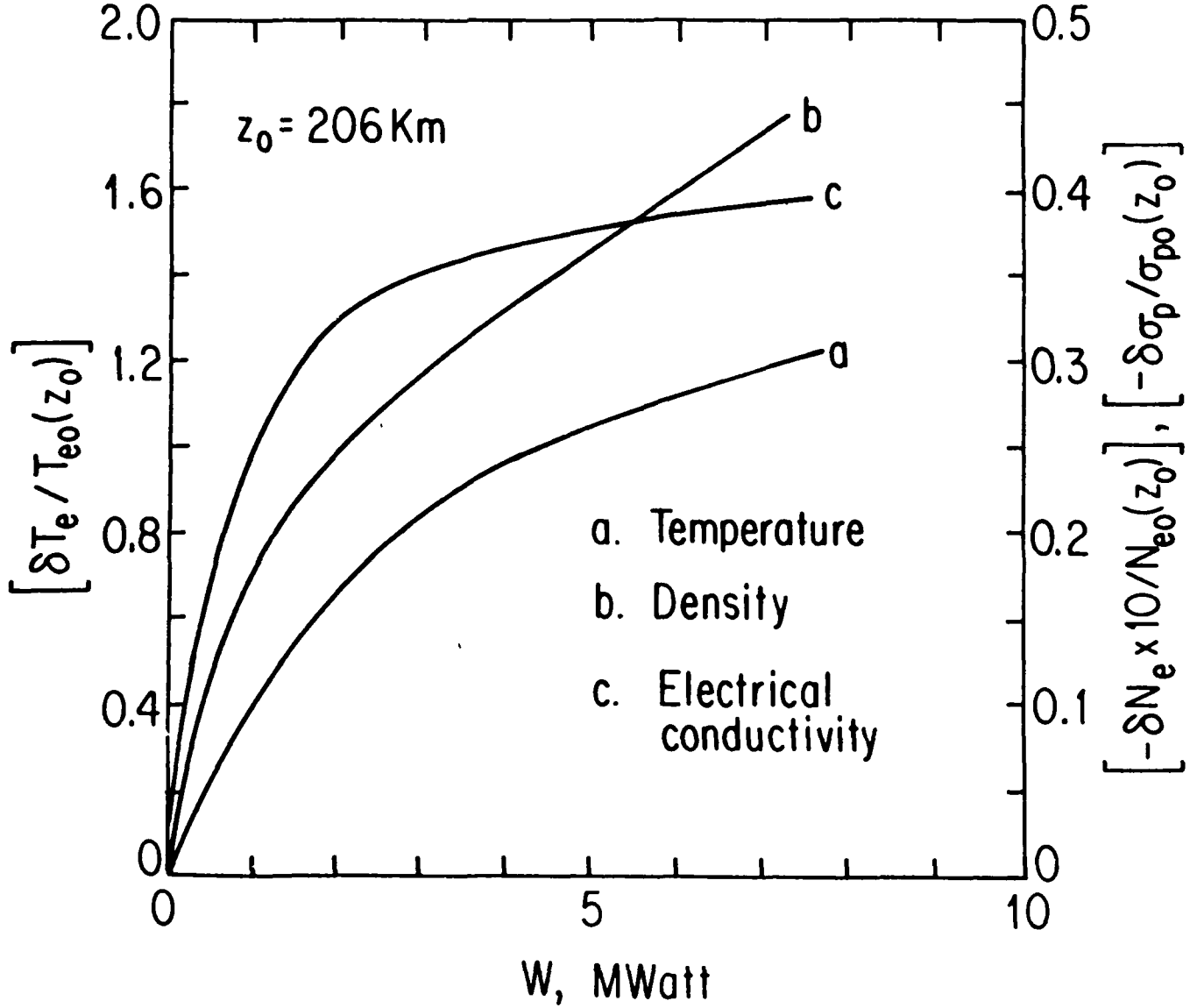
2.0
1.6
1.2
0.8
0.4
0
0.5
0.4
0.3
0.2
0.1
0
0
5
10
z_0 = 206 Km
b
c
a
a. Temperature
b. Density
c. Electrical conductivity
$[\delta T_e / T_{eo}(z_0)]$
$[-\delta N_e \times 10/N_{eo}(z_0)]$, $[-\delta\sigma_p/\sigma_{po}(z_0)]$
W, MWatt

Fig. 7

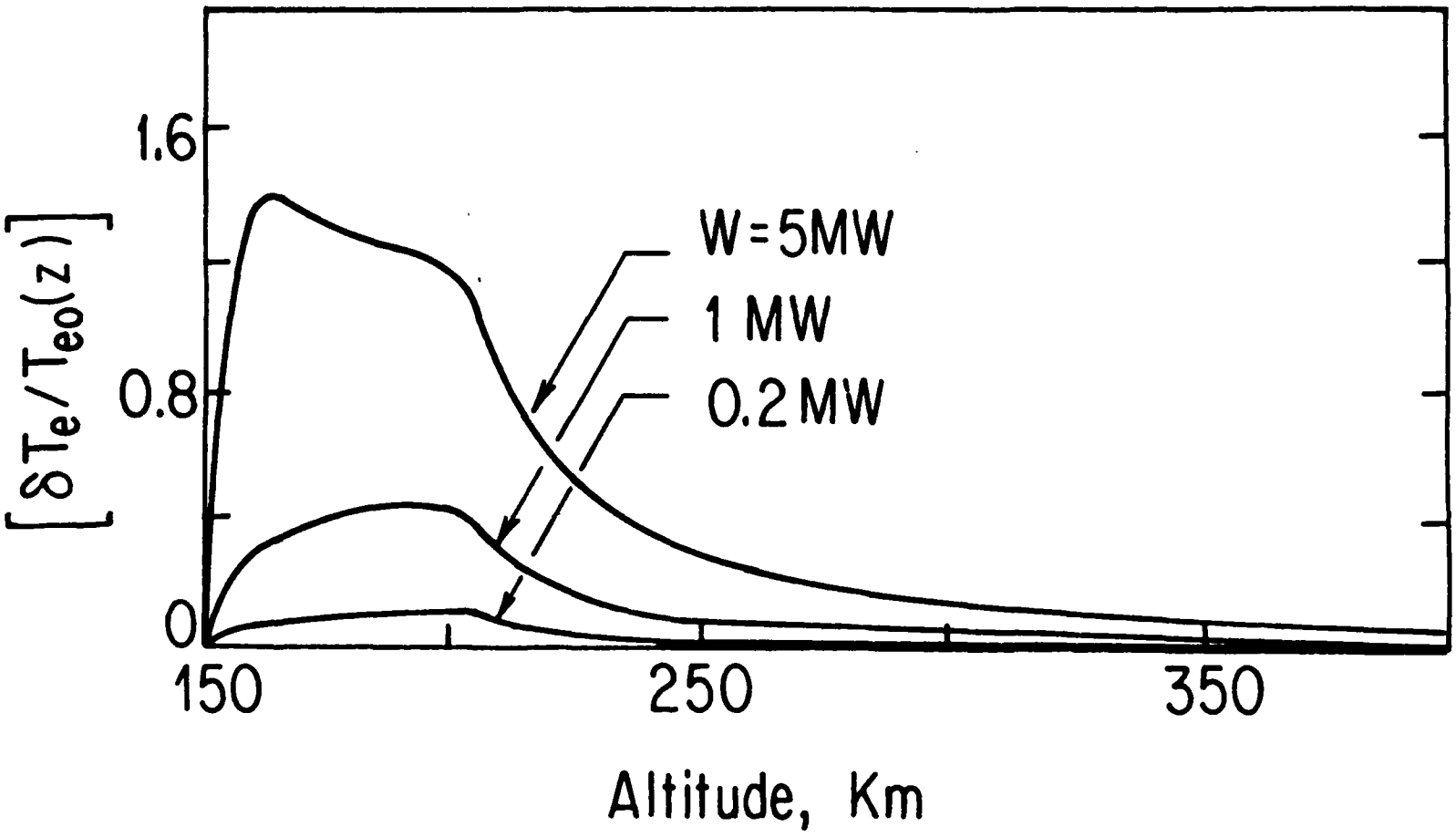

Fig. 8

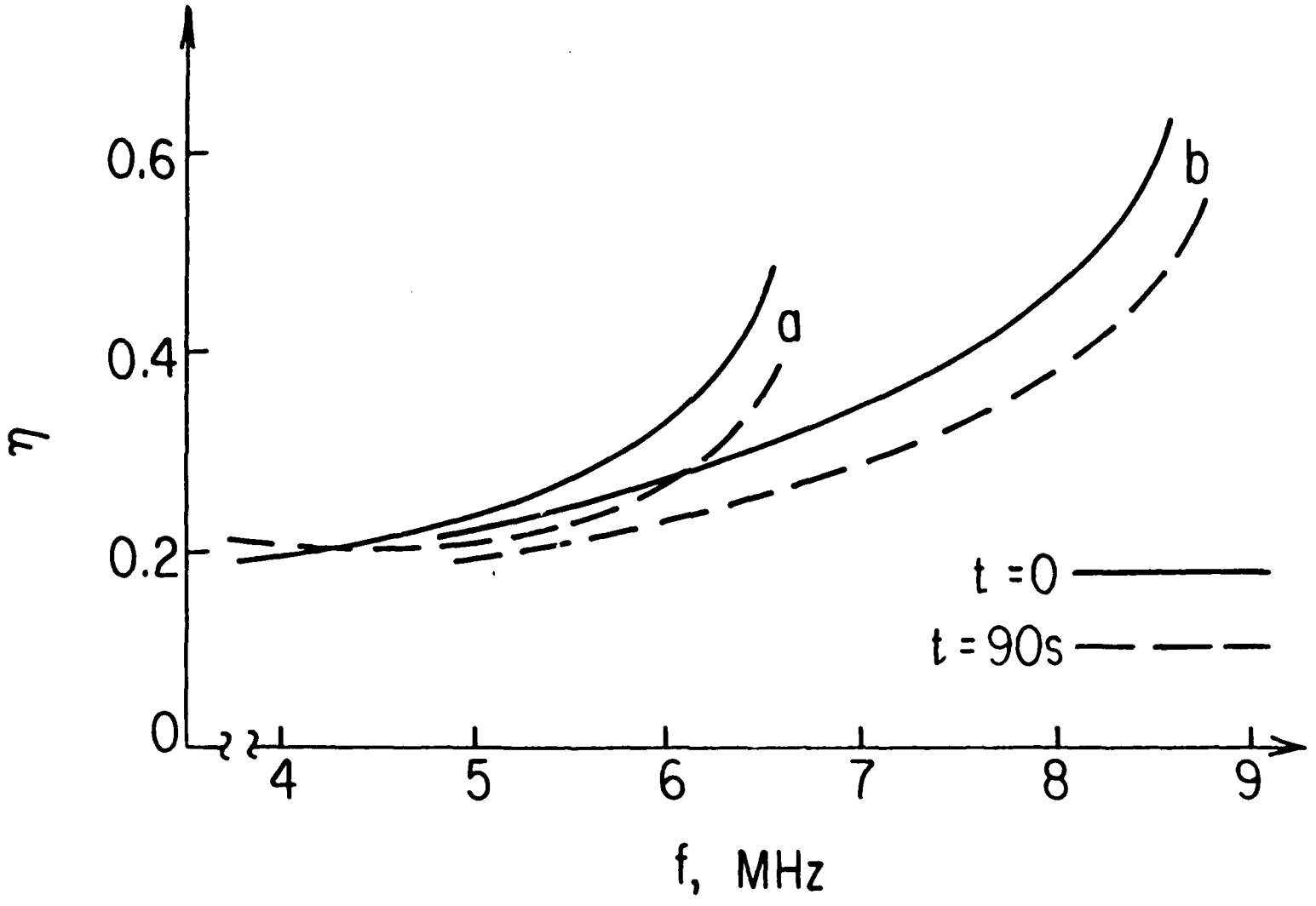

Fig. 9

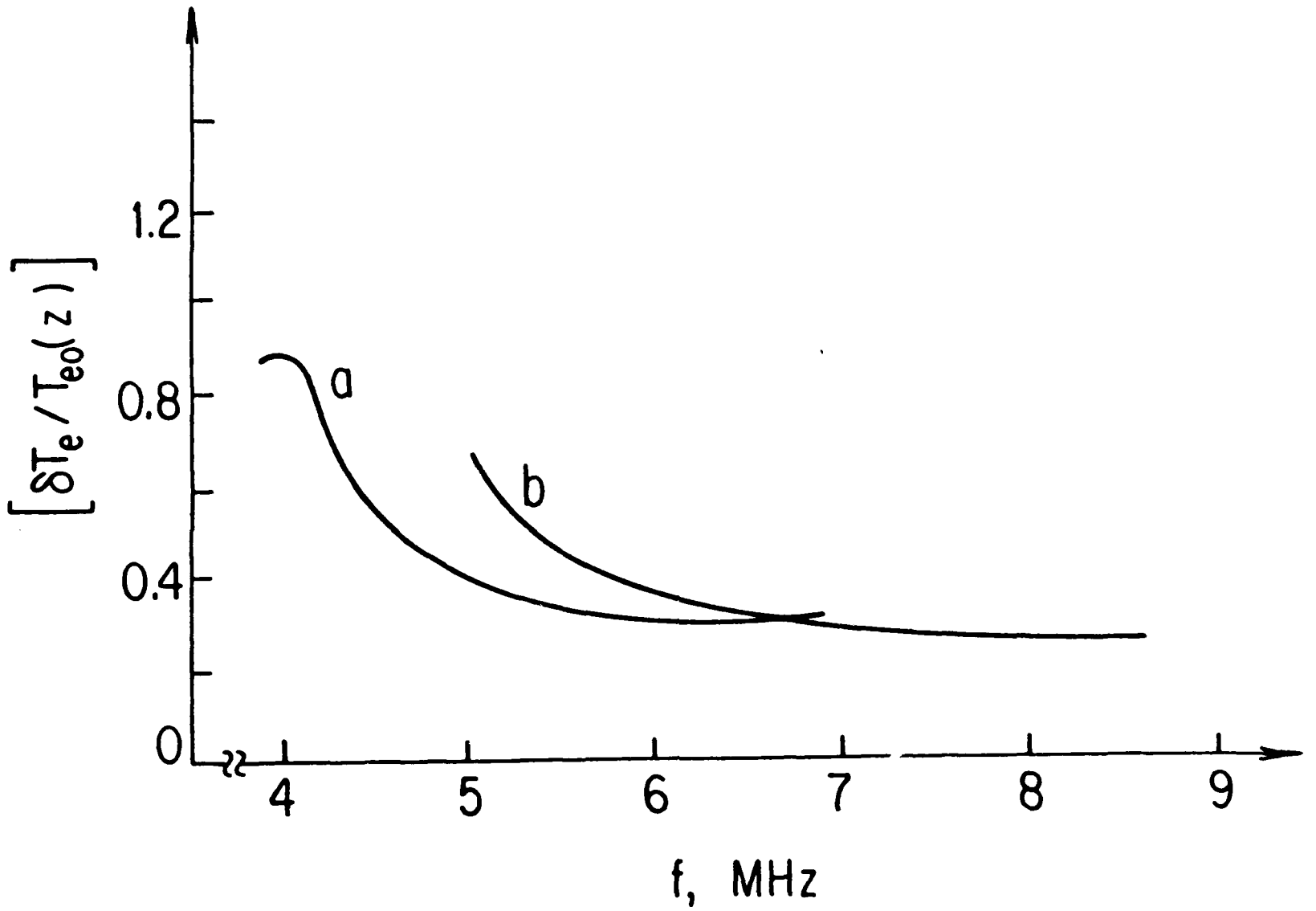

Fig. 10

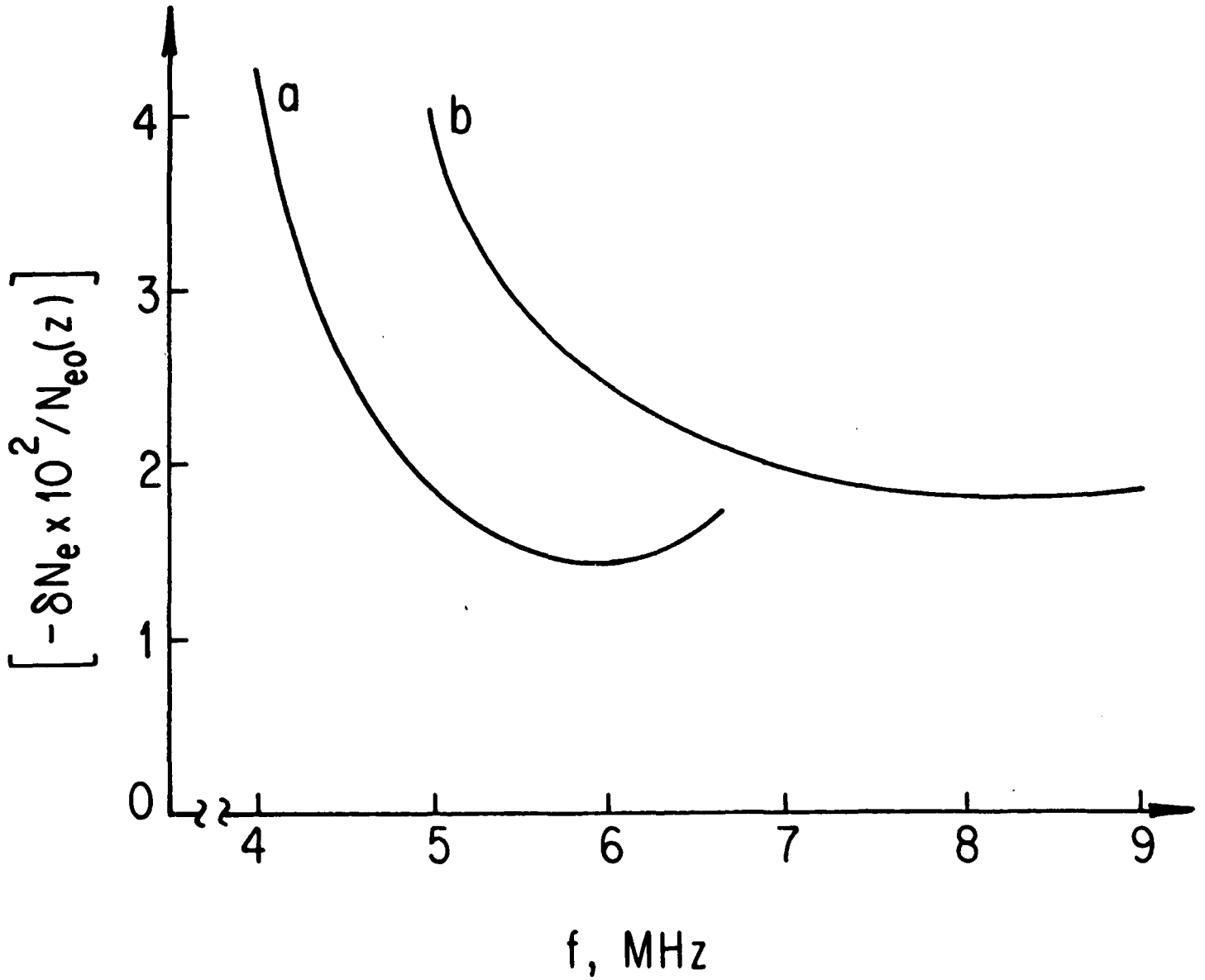

Fig. 11

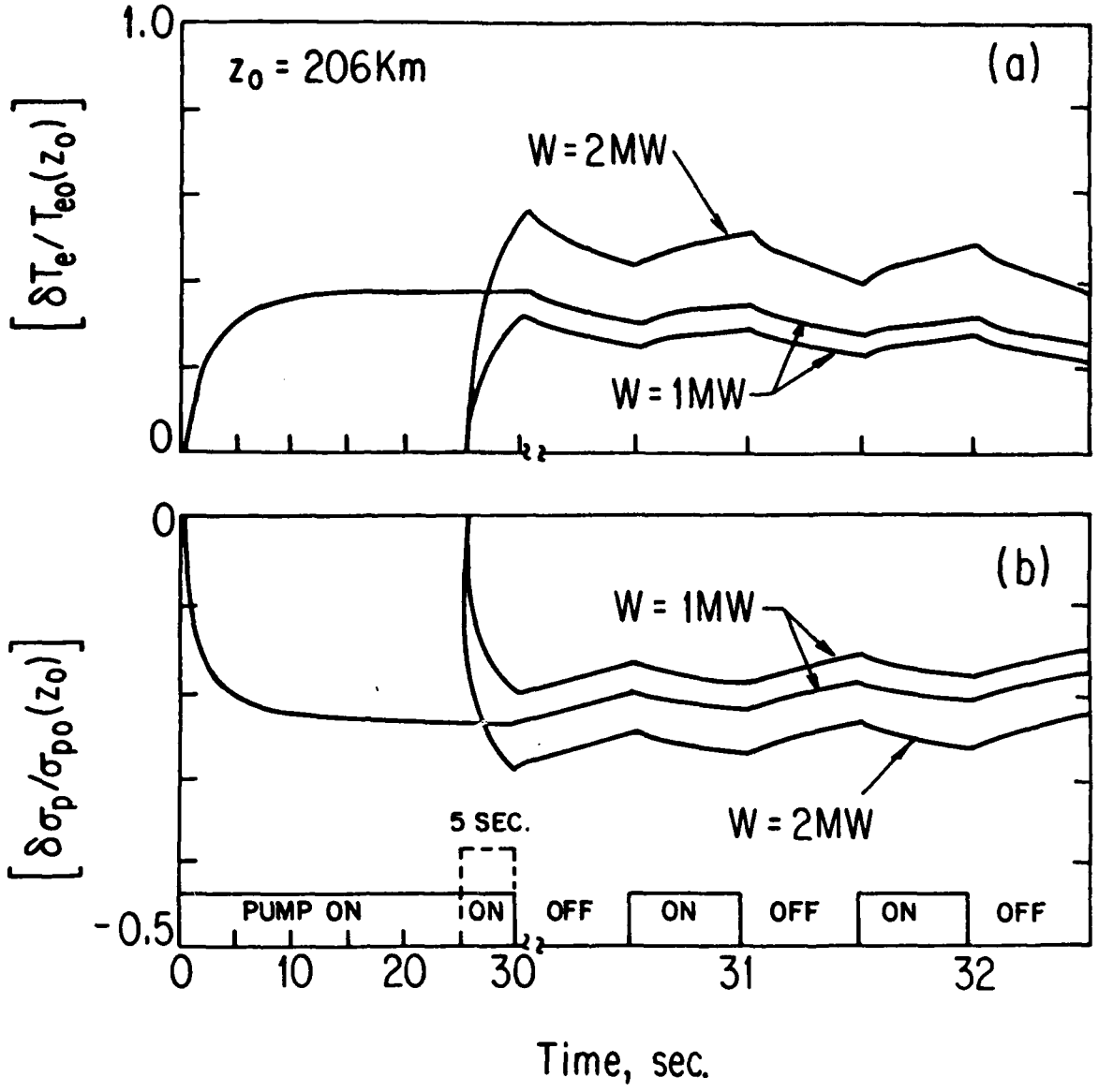
1.0
z_0 = 206Km
(a)
W = 2MW
W = 1MW
0
$[\delta T_e / T_{eo}(z_0)]$
0
(b)
W = 1MW
W = 2MW
5 SEC.
PUMP ON
ON
OFF
ON
OFF
ON
OFF
-0.5
$[\delta \sigma_p / \sigma_{po}(z_0)]$
0
10
20
30
31
32
Time, sec.

Fig. 12

PPG-734 "Containment of Laser Produced High Beta Plasmas by Relatively Weak Surface Magnetic Fields," A. Y. Wong, (August, 1983), submitted to Physical Review Letters.

PPG-735 "Thomson Scattering Measurements of Electron Power Losses in the UCLA Didecapole SURMAC," K. Jones, Ph.D. Dissertation, August 1983.

PPG-736 "Bounded, Electrostatic Particle Simulation Code on the UCLA CHI Computer System," V. K. Decyk.

PPG-737 "Magnetic Field Line Reconnection Experiments, Part 6 - Magnetic Turbulence", W. Gekelman & R. L. Stenzel, submitted to Jour. Geophys. Res., August 1983

PPG-738 "Accretion Disk Electrodynamics", F. V. Coroniti, August, 1983 for International Astronomical Union Symposium/ Highlights of Astronomy

PPG-739 "Neutron Radiation Effects on the Structure of the Particle Beam Fusion Target Development Facility," N. Ghoniem, not for publication, (August, 1983).

PPG-740 "Ion Trapping Saturation of the Brillouin Instability ", C. E. Clayton, C. Joshi, F. F. Chen, submitted to Phys. Rev. Lett., August 1983.

PPG-741 "Laboratory Experiments on Current Sheet Disruptions, Double Layers, Turbulence and Reconnection," by R. L. Stenzel, AGU Meeting, August, 1983.

PPG-742 "An Advanced Pump Limiter Experiment of Large Toroidal Extent--ALT 2," Bob Conn, et al., not for publication, August 1983.

PPG-743 "Constitutive Design Equations for Creep Deformation of HT-9," Robert Amodeo & Nasr Ghoniem, submitted to Journal of Nuclear Material, August, 1983.

PPG-744 "The Interaction of High Energy Collision Cascades with Helium Field Cavities and Carbide Precipitations," Philip Chou & Nasr Ghoniem, submitted to Journal of Nuclear Material, August, 1983.

PPG-745 "Behavior of the Ponderomotive Effect Near Gyroresonance", B. M. Lamb, G. Dimonte and G. J. Morales, submitted to Physics of Fluids, September 1983

PPG-746 "Collisional and Convective Thresholds for Ramen Backscatter", B. Amini, F. F. Chen, not for pub., September 1983.

PPG-747 "Observations of Lower Hybrid Noise in the Io Plasma Torus and Anomalous Plasma Heating Rates," D. D. Barbosa, F. V. Coroniti, W. S. Kurth & F. L. Scarf, Sept. 1983.

PPG-748 "Ohmic Heating of the Polar F-Region by HF Pulses," M. M. Shoucri & G. J. Morales, J. E. Maggs, submitted to JGR, October 1983.

END

FILMED

1-84

DTIC